Applied Radiation and Isotopes 135 (2018) 47–56

Contents lists available at ScienceDirect

Applied Radiation and Isotopes

journal homepage: www.elsevier.com/locate/apradiso

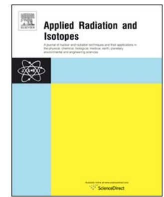

Temperature dependence of ^{63}Ni–Si betavoltaic microbattery

Liu Yunpeng[a,b], Guo Xiao[a], Jin Zhangang[a], Tang Xiaobin[a,b,*]

[a] Department of Nuclear Science and Engineering, Nanjing University of Aeronautics and Astronautics, Nanjing 210016, China
[b] Jiangsu Key Laboratory of Material and Technology for Energy Conversion, Nanjing 210016, China

HIGHLIGHTS

- Temperature dependence of ^{63}Ni–Si betavoltaic microbattery with different source conditions was studied.
- The higher the source thickness, activity, and energy, the lower is the betavoltaic performance responds to temperature.
- V_{oc} and P_{max} sensitivities of the interbedded betavoltaic with high-activity ^{63}Ni are lower than those of low-activity one.
- V_{oc} sensitivity of the interbedded betavoltaic in series is equal to the sum of those of the upper and lower ones.
- P_{max} sensitivity of the interbedded betavoltaic is the average of those of the upper and lower ones.

ARTICLE INFO

Keywords:
Betavoltaic
Temperature dependence
Apparent activity density
Energy conversion unit
Open-circuit voltage sensitivity
Maximum output power sensitivity

ABSTRACT

This paper theoretically presented the temperature effects on the ^{63}Ni–Si betavoltaic microbattery irradiated by a source with different thicknesses and activity densities at a temperature range 170–340 K. Temperature dependences of the monolayer and interbedded ^{63}Ni–Si betavoltaics at 213.15–333.15 K were tested with respect to calculations. Results showed that the higher the thickness, activity density, and average energy of the source, the lower is the betavoltaic performance responds to temperature. With the increase in temperature, the V_{oc} and P_{max} of the upper, lower, and interbedded betavoltaics decreased linearly at low temperatures and decreased exponentially at high temperatures in the experiment. As predicted, the measured V_{oc} and P_{max} sensitivities of the lower betavoltaic with 4.90 mCi/cm^2 ^{63}Ni, −2.230 mV/K and −1.132%, respectively, were lower than those with 1.96 mCi/cm^2 ^{63}Ni, −2.490 mV/K and −1.348%, respectively. Compared with the calculated results, the prepared betavoltaics had lower V_{oc} sensitivity and higher P_{max} sensitivity. In addition, the measured V_{oc} sensitivity of the interbedded betavoltaic in series is equal to the sum of those of the upper and lower ones as predicted. Moreover, the measured P_{max} sensitivity of the interbedded betavoltaic is equal to the average of those of the two monolayers.

1. Introduction

Betavoltaics are a type of nuclear batteries that store energy in a beta source, and this energy is converted to electricity when the beta particles interact with a semiconductor PN junction, thus forming electron–hole pairs (EHPs) that are drawn off as current (Olsen et al., 2012). With long lifetime, high energy density, and amenable to miniaturization, betavoltaics possess significant potential for use as next-generation microbatteries in microelectromechanical systems (Chen et al., 2012). Therefore, they have become worldwide research and development hotspots (Olsen et al., 2012; Luo et al., 2011).

A betavoltaic is composed of a beta source and a semiconductor junction energy conversion unit (ECU). The surrounding environments, such as temperature and vacuum, do not affect the beta source decay (Liu et al., 2014a; Liu et al., 2017). However, the characteristics, including the minority carrier property and reverse saturation current, of the ECU can be easily affected by the surrounding environments, especially temperature (Liu et al., 2017), which will affect the output performance consequently. Betavoltaic microbatteries can be essential in outer space, desert, arctic, and deep-sea applications. These environments have extreme temperature, and the temperature can vary over a wide range. Hence, it is necessary to study the temperature (T) dependence of betavoltaics (Butera et al., 2017a).

To fully understand the temperature dependence, the investigation can be separated into three aspects. First, it is the temperature effect on the electrical performance of betavoltaics, including short-circuit current (I_{sc}), open-circuit voltage (V_{oc}), maximum output power (P_{max}), fill factor (FF), energy conversion efficiency (η), and reverse saturation

* Corresponding author at: Department of Nuclear Science and Engineering, Nanjing University of Aeronautics and Astronautics, Nanjing 210016, China.
E-mail address: tangxiaobin@nuaa.edu.cn (T. Xiaobin).

https://doi.org/10.1016/j.apradiso.2018.01.017
Received 2 August 2017; Received in revised form 15 November 2017; Accepted 12 January 2018
0969-8043/ © 2018 Elsevier Ltd. All rights reserved.

current (I_0). Most of previous studies about betavoltaics based on ^{3}H–GaAs (Cheu et al., 2017; Adams et al., 2016), ^{63}Ni–Si (Liu et al., 2014a; Wang et al., 2015; Liu et al., 2014a; Wang et al., 2010; Ghasemi et al., 2014), ^{63}Ni–GaAs (Butera et al., 2017a; Wang et al., 2015), ^{63}Ni–AlInP (Butera et al., 2016), ^{63}Ni–InGaP(GaInP) (Butera et al., 2017b), ^{63}Ni–4H–SiC (Chandrashekhar et al., 2007), ^{147}Pm-Si (Wang et al., 2015), ^{147}Pm–GaAs (Wang et al., 2015), and ^{55}Fe–InGaP (GaInP) (Butera et al., 2017c) have involved this part work. Second, it is the temperature effect on the characteristic parameters of semiconductor materials including bandgap, intrinsic carrier concentration, carrier lifetime, diffusion length, and mobility. Cheu et al. (2017) discussed the variations in bandgap to estimate the V_{oc} sensitivity at various temperatures of −30 to 70 °C. Wang et al. (2010) and Chandrashekhar et al. (2007) predicted the V_{oc} sensitivity by calculating the temperature dependence of intrinsic carrier concentration and minority carrier lifetime. Ghasemi et al. (2014) simulated the temperature effects on minority carrier characteristics to obtain the electrical performances of the betavoltaic at 150–500 K. Finally, it is the relationship between the structural parameters of betavoltaics, such as the type of source, average energy of apparent emitted particles, activity of source, type of semiconductor, doping concentration, junction depth, connection type of ECUs, and the temperature characteristic. Ghasemi et al. (2014) studied the V_{oc} temperature dependence of betavoltaics irradiated by ^{63}Ni beta sources with various activities and different junction depths theoretically but did not measure it experimentally. Our previous studies were on the electrical performances of betavoltaics and parameters of semiconductor. We also discussed the effects of sources (^{63}Ni and ^{147}Pm) and ECUs (Si and GaAs) on temperature dependence. Moreover, we studied the temperature effects on an interbedded-structure betavoltaic in series (Liu et al., 2014a; Wang et al., 2015; Liu et al., 2014b).

In this paper, we studied the temperature dependence of the electrical performances of the monolayer-structure Si betavoltaic irradiated by ^{63}Ni with various activities. We then compared the temperature dependences between the monolayer- and interbedded-structure ^{63}Ni–Si betavoltaics both experimentally and theoretically. In addition, we analyzed the bandgap, intrinsic carrier concentration, minority diffusion length, and the effect of the average energy of the emitted particles from ^{63}Ni at 213.15–333.15 K. This work can help in more deeply understanding the temperature characteristic of betavoltaics.

2. Materials and methods

2.1. Radioisotope sources and semiconductor materials

2.1.1. Materials in the theoretical calculation

Radioisotope beta source ^{63}Ni and semiconductor Si were used to explore the temperature effects on betavoltaic theoretically. The apparent activity density and apparent average energy of the particles emitted from sources of different thicknesses can be obtained by using the Monte Carlo code MCNP5 with the simulation method described by Liu et al. (2015). During this theoretical calculation, two types of ^{63}Ni, one with different thicknesses and the other with different apparent activity densities, were used to discuss the temperature dependence. For ^{63}Ni with different thicknesses, as shown in Table 1, the isotopic abundance of ^{63}Ni was set to 100%, and the apparent average energies were slightly different from each other because of the self-absorption effect (Liu et al., 2015). For ^{63}Ni with different apparent activity densities, as shown in Table 2, the isotopic abundance of ^{63}Ni was not a constant but lower than 100%. These two types of sources having the same activity density differ in their average energies; hence, the effect of average energy on the temperature dependence of betavoltaics could be evaluated.

Table 1
Parameters of ^{63}Ni with different thicknesses in the theoretical calculation.

Thickness (μm)	Apparent activity density (mCi/cm^2)	Apparent average energy (keV)
0.0445	1	18.443
0.293	5	20.532
0.888	10	22.314
2	13.23	23.234

Table 2
Parameters of ^{63}Ni with different apparent activity densities in the theoretical calculation.

Thickness (μm)	Apparent activity density (mCi/cm^2)	Apparent average energy (keV)
6	1	23.422
6	5	23.422
6	10	23.422
6	13.23	23.422

2.1.2. Materials in the experiment

An N-type silicon substrate wafer with doping concentration of 9.3 × 10^{13} /cm^3 and thickness of 300 μm was used to prepare the ECUs. ECUs with front peak B^+ doping of 3.3 × 10^{19} /cm^3, junction depth of 0.68 μm, and back peaking P^+ doping of 7.7 × 10^{19} /cm^3 of the betavoltaic were manufactured by ion implantation and conventional thermal annealing. Table 3 shows the layer details of the Si ECU. The active area of the ECU was 0.5 × 0.5 cm^2 with an external size of 0.7 × 0.7 cm^2.

Table 3
Layer details of the Si ECU.

Layer	Material	Thickness (μm)	Dopant	Dopant type	Dopant density (/cm^3)
1	Al	1			
2	Si	0.68	B	P^+	3.3 × 10^{19}
3	Substrate Si	300	P	N^-	9.3 × 10^{13}
4	Si		P	N^+	7.7 × 10^{19}
5	Al	1			

Two ECUs, namely the upper and the lower ECUs, assembled themselves into an interbedded-structure betavoltaic with a bidirectional radioisotope ^{63}Ni. The apparent activity density of one side of the bidirectional ^{63}Ni is 4.90 mCi/cm^2. The lower ECU and a one-sided ^{63}Ni of 1.96 mCi/cm^2 constituted the monolayer-structure betavoltaic. The effect of activity on the temperature characteristic could be estimated from those of high- and low-activity density ^{63}Ni in the experiment. Table 4 shows the betavoltaic samples and radioisotopes of ^{63}Ni. In addition, both the bidirectional ^{63}Ni and one-sided ^{63}Ni are disc shaped with an internal diameter of 2.5 cm, that is, the active area, and an external diameter of 3 cm.

Table 4
Betavoltaic samples and radioisotopes of ^{63}Ni in the experiment.

Samples	ECUs	Beta source	Apparent activity density (mCi/cm^2)
Interbedded-structure betavoltaic	Upper and lower	Bidirectional ^{63}Ni	4.90
Monolayer-structure betavoltaic	Lower	One-sided ^{63}Ni	1.96

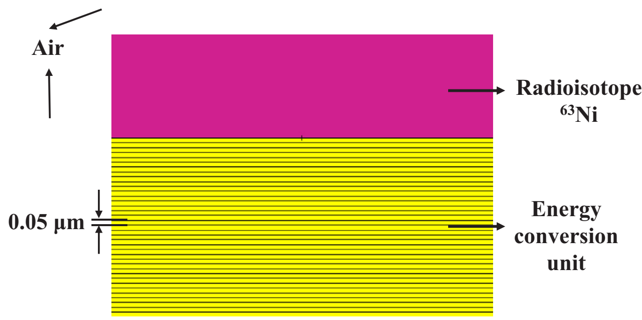

Fig. 1. Calculation monolayer model of ^{63}Ni–Si betavoltaic microbattery used to study the temperature dependence using MCNP5.

2.2. Calculation methods in theory

2.2.1. Calculation model for temperature dependence

As shown in Fig. 1, the calculation monolayer model of ^{63}Ni–Si betavoltaic microbattery used to study the temperature dependence in theory was established using the Monte Carlo code MCNP5. In this part, we theoretically and abstractly study the temperature dependence to show the universal law. Therefore, some simplifications were made. ^{63}Ni was located above the ECU without any air gap. The parameters of ^{63}Ni are provided in Tables 1, 2. The ECU uses a group of optimized structural parameters with a P-type substrate of $N_A = 5.62 \times 10^{17}$/cm^3, surface doped area of $N_D = 7.08 \times 10^{19}$/cm^3, junction depth of 0.05 µm, and thickness of 28 µm (Liu et al., 2014b). The betavoltaic is one kind of square cell with a cross-sectional area of 1 × 1 cm^2. Deposition layers with 0.05 µm thickness could count the electron–holes pairs (EHPs) at any depth of the Si ECU.

2.2.2. Empirical formulas for performances as a function of temperature

In general, semiconductor material parameters such as bandgap, intrinsic carrier concentration, mobility, lifetime, and diffusion length vary with temperature and thus alter the electrical performances of betavoltaics. As the temperature increases, the lattice spacing becomes larger and, consequently, the energy-band width decreases. For semiconductor materials, one atomic energy level does not equal one energy band; hence, the bandgap decreases with the increase in temperature. The bandgap (E_g) as a function of temperature is usually given by the following empirical formula:

$$E_g(T) = E_g(0) - C_1 T^2/(T + C_2) \quad (1)$$

where $E_g(0)$ is the bandgap at absolute zero Kelvin ($E_g(0) = 1.17$ eV for Si), C_1 and C_2 are the constants for the specified materials ($C_1 = 4.73 \times 10^{-4}$ eV/K and $C_2 = 636$ K for Si (Li, 1993)), and T is the temperature in Kelvin. The following formula shows the relationship between the intrinsic carrier concentration (n_i) and T (Misiakos and Tsamakis, 1993).

$$n_i(T) = 5.29 \times 10^{19}(T/300)^{2.54}\exp(-6726/T) \quad 78\text{~}340\ \text{K} \quad (2)$$

Empirical formulas of minority carrier mobility (μ) and minority carrier lifetime (τ) as a function of temperature were provided by Reggiani et al. (2000) and Klaassen (1992), respectively. The temperature dependence of minority diffusion length (L) can then be derived by the equation $L = \sqrt{(kT/q)\mu\tau}$. The number of electron–hole pairs at any depth of the Si ECU was counted by the 0.05-µm deposition layers with *F8 count card. Moreover, the electrical performances including the short-circuit current density (J_{sc}), V_{oc}, P_{max}, and FF of the betavoltaic were obtained every 10 K from 170 to 340 K by using the calculation method used in our previous study (Liu et al., 2014b).

The V_{oc} sensitivity refers to the reduced value as the temperature increases one degree, and its unit is mV/K. The P_{max} sensitivity refers to the reduced percentage with respect to the value at the reference temperature as the temperature increases one degree, and its unit is %/K. The following two formulas give the V_{oc} and P_{max} sensitivities, respectively.

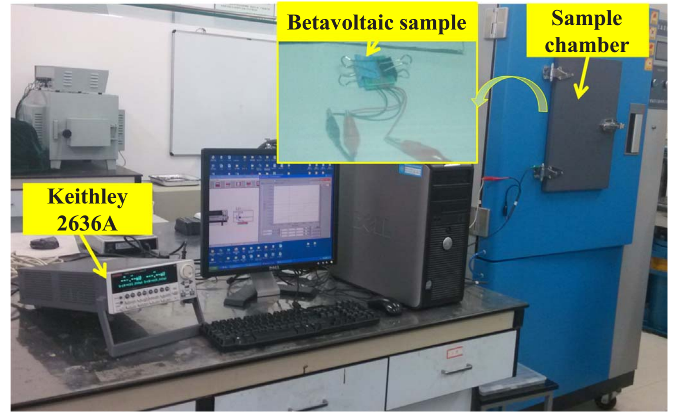

Fig. 2. Measurement schematic for the interbedded-structure betavoltaic in series and the monolayer-structure ^{63}Ni–Si betavoltaics.

$$\frac{dV_{oc}}{dT} = d\left(\frac{kT}{q}\ln\left(\frac{J_{sc}}{J_0} + 1\right)\right)/dT \quad (3)$$

$$\frac{1}{P_{\max}}\frac{dP_{\max}}{dT} = \frac{1}{V_{oc}}\frac{dV_{oc}}{dT} + \frac{1}{FF}\frac{dFF}{dT} + \frac{1}{J_{sc}}\frac{dJ_{sc}}{dT} \quad (4)$$

2.3. Experimental measurement methods

The temperature effects on betavoltaic were measured at ordinary pressure and 50% humidity in the high–low temperature test chamber (Shandong Drick Instruments Co., Ltd., China, model: DRK641A) as shown in Fig. 2. The I–V characteristics of betavoltaics, including the upper monolayer, lower monolayer, and interbedded cells, were measured every 10 K in the range of 213.15–333.15 K using a Keithley 2636 A source meter. For the interbedded-structure betavoltaic, the upper and lower ECUs were connected in series. The dark current as a function of reverse bias for these betavoltaics was also measured without ^{63}Ni irradiation. In addition, a 0.7-mm air gap was provided between ^{63}Ni and the upper or lower ECUs in the experiment to avoid the ^{63}Ni slice touching the down leads and causing short circuit or fracture.

2.4. Calculation model for comparing the measured results

According to the practical structural parameters of the betavoltaic samples in the experiment, such as source thickness, ECU thickness,

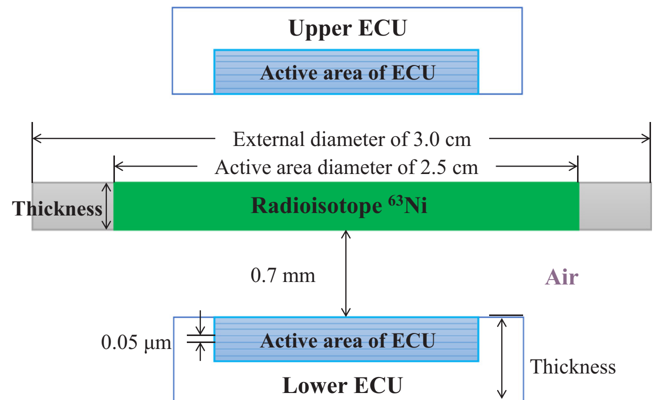

Fig. 3. Calculation model of temperature dependence used to compare the measured results using the MCNP5.

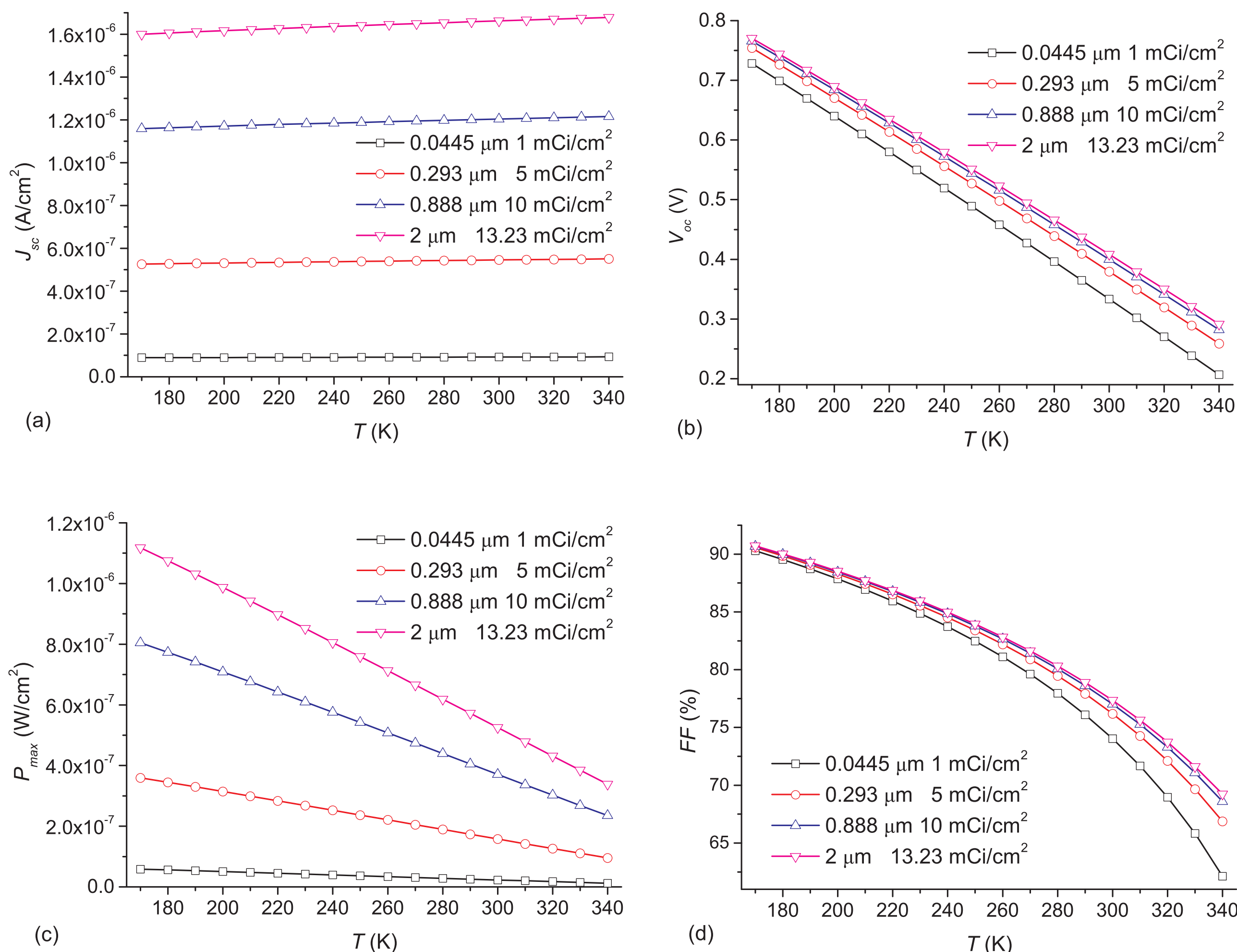

Fig. 4. Changes in (a) J_{sc}, (b) V_{oc}, (c) P_{max}, and (d) FF as a function of temperature for different thicknesses of ^{63}Ni.

junction depth, doping concentration, and air gap, the calculation model was established to simulate the electrical performances and compare the measured results by using the MCNP5 code, as shown in Fig. 3. This model is different from that in Fig. 1. The upper ECU has the same thickness of 300 μm as the lower ECU. The active area of the ECU was 0.5 × 0.5 cm^2 with an external size of 0.7 × 0.7 cm^2 and thickness of 28 μm. The ECU was divided into 560 counting layers each with a thickness of 0.05 μm. In addition, the air gap was 0.7 mm with a density of 1.1619 × 10^{-3} g/cm^3. The PN junction depth almost contained 14 counting layers with 0.7 μm thick, to simulate the actual 0.68 μm depth. The doping densities for N_A and N_D were set on the basis of the prepared samples.

For the interbedded betavoltaic in series, the thickness of ^{63}Ni was set to 0.293 μm on the basis of the apparent activity density of 4.90 mCi/cm^2, as shown in Table 4 (the factory apparent activity density was 5 mCi/cm^2). For the monolayer betavoltaic, the calculation model involved only the one-sided ^{63}Ni and the lower ECU without the upper ECU, as shown in Fig. 3. The thickness of ^{63}Ni was set to 0.095 μm on the basis of the apparent activity density of 1.96 mCi/cm^2, as shown in Table 4 (the factory apparent activity density was 2 mCi/cm^2).

3. Results

3.1. Calculated results

3.1.1. Calculated results for beta sources with different thicknesses

Fig. 4 shows the changes in J_{sc}, V_{oc}, P_{max}, and FF as a function of temperature for different thicknesses of ^{63}Ni. With the increase in temperature, the change trends of the aforementioned four parameters were similar to each other. The value of J_{sc} increased gently, V_{oc} and P_{max} decreased linearly, and FF decreased regularly with the increase in temperature.

However, the variation extents of the electrical performances were not similar to each other for ^{63}Ni of different thicknesses. Table 5 shows the V_{oc} and P_{max} sensitivities, in which the latter is with respect to the value at 300 K. With the increase in source thickness, the V_{oc} and P_{max} sensitivities both decreased.

3.1.2. Calculated results for beta sources with different apparent activities

Fig. 5 shows the changes in J_{sc}, V_{oc}, P_{max}, and FF as a function of temperature for different apparent activity densities of ^{63}Ni. The four parameters showed a similar varying tendency with the increase in temperature. J_{sc} increased gently, V_{oc} and P_{max} decreased linearly, and FF decreased regularly with the increase in temperature.

However, the extent of changes in the electrical performances is different for ^{63}Ni with various apparent activity densities. Table 6

Table 5
V_{oc} and P_{max} sensitivities of betavoltaic irradiated by ^{63}Ni of various thicknesses.

Thickness of ^{63}Ni (μm)	Apparent activity density (mCi/cm^2)	V_{oc} (mV/K)	P_{max} (%/K)
0.0445	1	−3.068	−1.203
0.293	5	−2.914	−0.984
0.888	10	−2.846	−0.904
2	13.23	−2.818	−0.873

Fig. 5. Changes in (a) J_{sc}, (b) V_{oc}, (c) P_{max}, and (d) FF as a function of temperature for different apparent activity densities of ^{63}Ni.

Table 6
V_{oc} and P_{max} sensitivities of betavoltaic irradiated by ^{63}Ni of various apparent activity densities.

Thickness of ^{63}Ni (μm)	Apparent activity density (mCi/cm^2)	V_{oc} (mV/K)	P_{max} (%/K)
6	1	−3.040	−1.154
6	5	−2.901	−0.965
6	10	−2.841	−0.897
6	13.23	−2.817	−0.872

shows the V_{oc} and P_{max} sensitivities of betavoltaic, in which the latter is with respect to the value at 300 K. The V_{oc} and P_{max} sensitivities both decreased with the increase in source thickness.

In addition, the V_{oc} and P_{max} sensitivities of 6-μm ^{63}Ni, which are shown in Table 6, were lower than those of 0.0445-, 0.293-, 0.888-, and 2-μm ^{63}Ni with the same apparent activity density, which are shown in Table 5. These results indicate that the temperature effects on betavoltaic with high apparent average energy ^{63}Ni are less significant than those on the betavoltaic with low energy at the same apparent activity density. Not only the activity density but also the average energy should be considered while discussing the temperature dependence of the betavoltaics.

3.2. Comparison of measured and calculated results

Fig. 6 shows the dark current as a function of reverse bias for the upper, lower, and interbedded ECUs at 300 K. At the same reverse bias

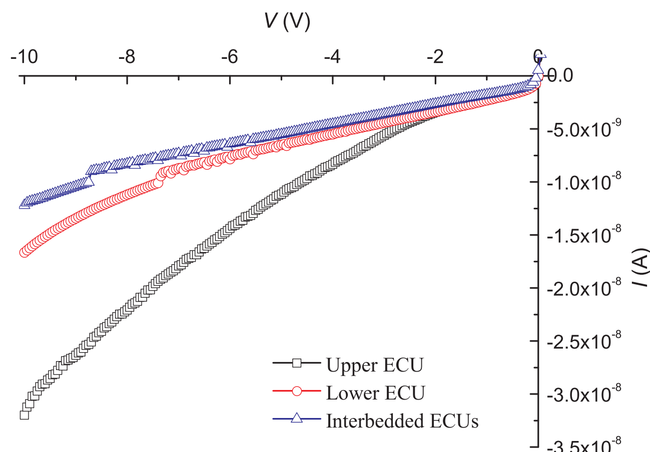

Fig. 6. Dark current as a function of reverse bias for the upper, lower, and interbedded ECUs at 300 K.

voltage, the dark current of the interbedded ECUs was lower than those of both the upper and lower ECUs, and the upper ECU had the highest value. The dark current of the upper, lower, and interbedded ECUs were -3.20×10^{-8}, -1.66×10^{-8}, and -1.22×10^{-8} A at -10 V bias, respectively.

Figs. 7 and 8 show the measured *I–V* characteristics of the upper, lower, and interbedded betavoltaics irradiated by 4.90 mCi/cm^2 bidirectional ^{63}Ni and those of the lower monolayer betavoltaic irradiated

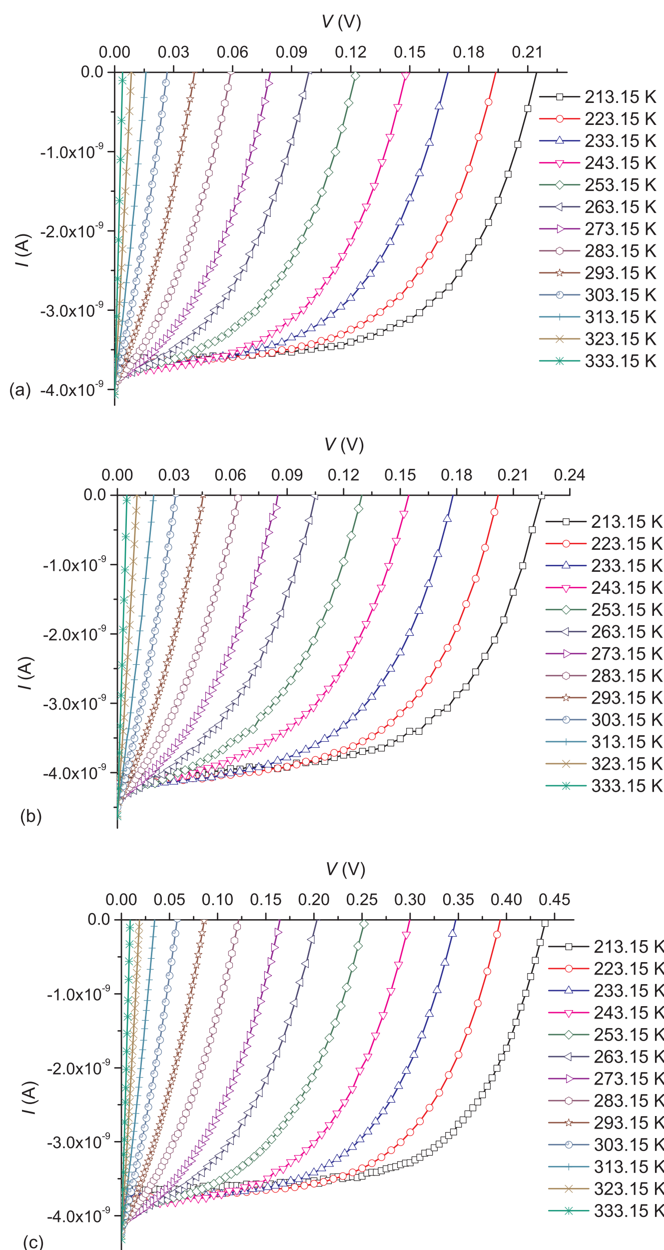

Fig. 7. Measured *I–V* characteristics of the (a) upper, (b) lower, and (c) interbedded betavoltaics irradiated by 4.90 mCi/cm^2 bidirectional ^{63}Ni at various temperatures.

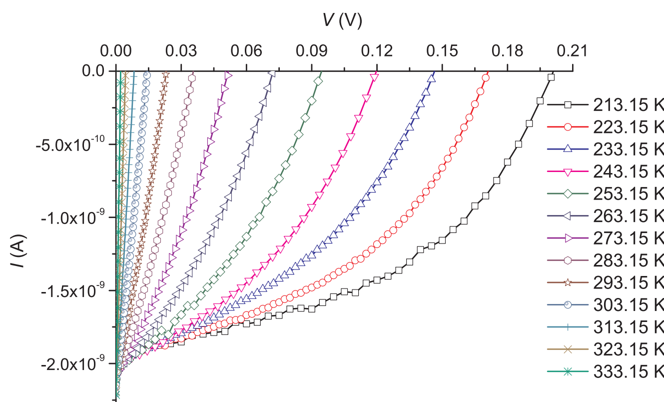

Fig. 8. Measured *I–V* characteristics of the lower monolayer betavoltaic irradiated by 1.96 mCi/cm^2 one-sided ^{63}Ni at various temperatures.

by 1.96 mCi/cm^2 one-sided ^{63}Ni at various temperatures, respectively. For these four *I–V* curves, the change trends were similar to each other with the increase in temperature. The inverse of the slope of the *I–V* curve at the open-circuit voltage point, that is, series resistance, decreased gradually. The inverse of the slope of the *I–V* curve at the short circuit current point, that is, shunt resistance, also decreased gradually with the increase in temperature.

Fig. 9 illustrates the measured changes in J_{sc}, V_{oc}, P_{max}, and FF as a function of temperature for the upper, lower, interbedded, and lower monolayer betavoltaics irradiated by different activity densities of ^{63}Ni. Fig. 10 shows the corresponding calculated results by using the model in Fig. 3. As shown in Fig. 9, the V_{oc}, P_{max}, and FF decreased remarkably, while J_{sc} increased slowly with the increase in temperature, which is in good agreement with the calculations in Fig. 10. In the experiment, the V_{oc} and P_{max} of the upper, lower, and interbedded betavoltaics with 4.90 mCi/cm^2 ^{63}Ni decreased linearly at low temperatures of 213.15–293.15 K and decreased exponentially at high temperatures of 293.15–333.15 K. Similarly, the V_{oc} and P_{max} of the lower monolayer betavoltaic with 1.96 mCi/cm^2 ^{63}Ni decreased linearly in the range 213.15–273.15 K and decreased exponentially in the range 273.15–333.15 K. However, in the calculation, the V_{oc} and P_{max} always decreased linearly at both low and high temperatures, as shown in Fig. 10.

In addition, the conversion efficiency of the upper betavoltaic with 4.90 mCi/cm^2 ^{63}Ni decreased from 0.315% to 0.003% as the temperature increased from 213.15 to 333.15 K in the experiment. For the lower one, it decreased from 0.365% to 0.004%, and for the interbedded one, from 0.337% to 0.003%. It decreased from 0.297% to 0.002% for the lower one with 1.96 mCi/cm^2 ^{63}Ni. The conversion efficiency is a term that is similar to P_{max}. Both have the same temperature dependence. Therefore, this study discussed the temperature effect on P_{max} alone. Wang et al. (2010) obtained larger efficiencies of 0.00975% and 0.265% for ^{63}Ni–Si Devices 0 and 1 at 333.15 K because of the higher activity of ^{63}Ni with 8 mCi.

Linear fitting the T–V_{oc} and T–P_{max} curves as shown in Figs. 9b and 9c at 213.15–293.15 K provided the measured V_{oc} and P_{max} sensitivities of the monolayer and interbedded betavoltaics, respectively. Moreover, the calculated V_{oc} and P_{max} sensitivities were also obtained by linear fitting the curves as shown in Figs. 10b and 10c at 213.15–333.15 K, respectively. Tables 7, 8 show these measured and calculated results irradiated by different activity densities of ^{63}Ni, in which the P_{max} sensitivity is with respect to the maximum output power at 213.13 K.

For the interbedded-structure in Table 7, as predicted in the calculation, the measured V_{oc} sensitivity of the interbedded betavoltaic in series was equal to the sum of those of the upper and lower monolayer ones. Moreover, the measured P_{max} sensitivity of the interbedded one was equal to the average of those of two monolayer ones. By comparing the results in Tables 7, 8, the measured V_{oc} and P_{max} sensitivities for the low-activity density source exceeded those for the high-activity density one, respectively. These results are in reasonable agreement with the related calculations. In addition, the measured V_{oc} sensitivities for all the betavoltaics were smaller than the theoretical ones, while the measured P_{max} sensitivities were larger than the theoretical ones irradiated by 4.90 mCi/cm^2 or 1.96 mCi/cm^2 ^{63}Ni.

4. Discussions

4.1. Temperature dependence of J_{sc}

The value of short circuit current density mainly depends on the number and collection efficiency of EHPs generated. In general, J_{sc} is an inverse function of bandgap. E_g significantly affects the number of EHPs. As shown in formula 1, E_g declined slightly as the temperature increased, which made the average energy to generate an EHP smaller than before. Consequently, the number of EHPs generated increased, so did the value of J_{sc}. However, it was very marginal as can be seen from

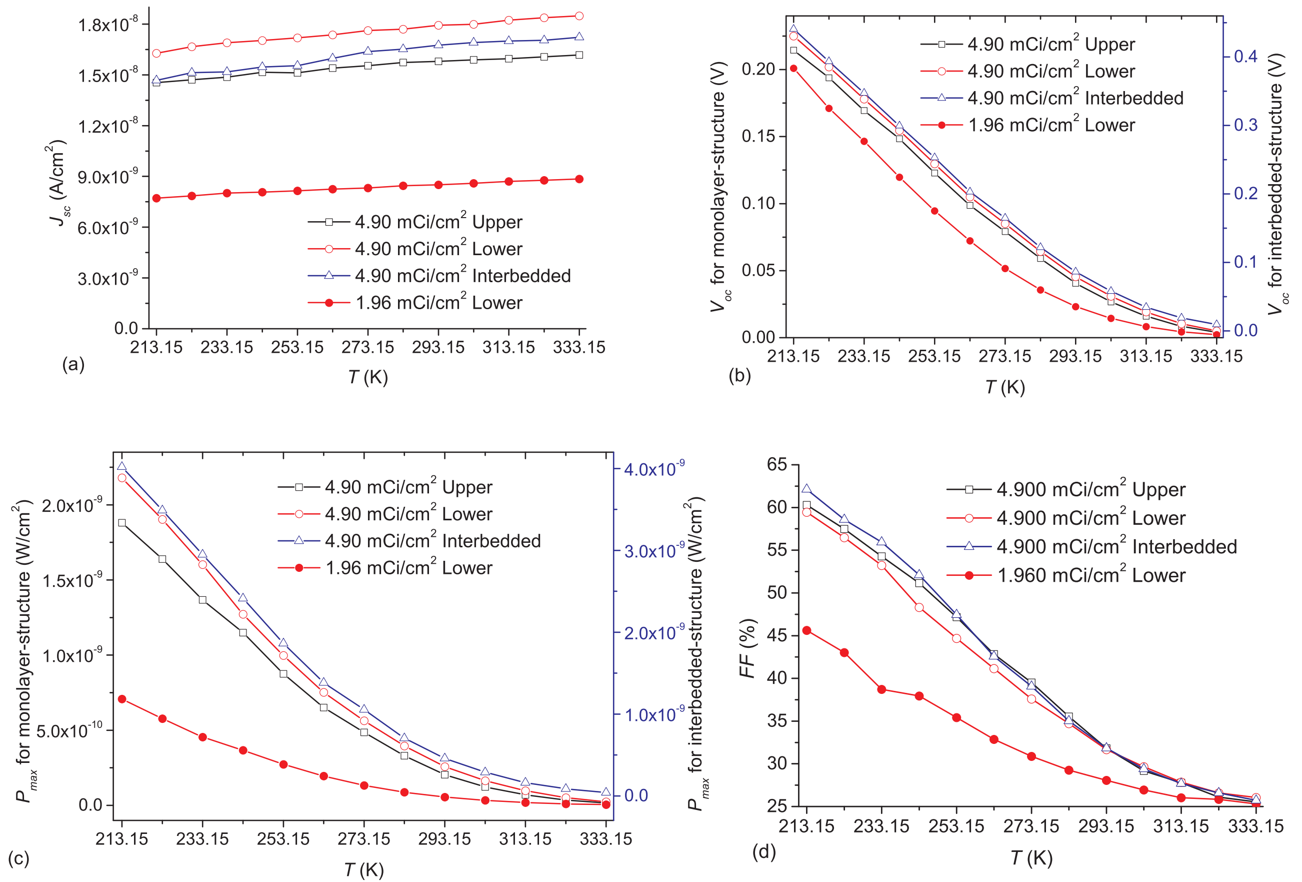

Fig. 9. Measured changes in (a) J_{sc}, (b) V_{oc}, (c)P_{max}, and (d) *FF* as a function of temperature for the upper, lower, interbedded betavoltaics irradiated by 4.90 mCi/cm^2 bidirectional ^{63}Ni and for the lower monolayer betavoltaics irradiated by 1.96 mCi/cm^2 one-sided ^{63}Ni, respectively.

Figs. 4, 5, 9, and 10 both in experiment and in calculation. This was mainly due to the decrease in the minority carrier diffusion in the surface heavily doping region and substrate region, as shown in Fig. 11, but these variations are not large. From the above analysis, it can be concluded that J_{sc} of both interbedded and monolayer betavoltaics increased slightly with the increase in temperature.

4.2. Temperature dependences of V_{oc} and P_{max}

For the prepared ^{63}Ni–Si betavoltaics, $N_D = 9.3 \times 10^{13}$/cm^3 of the lightly doping region, that is, the substrate region, is much lesser than $N_A = 3.3 \times 10^{19}$ /cm^3 of the surface heavily doping region. Hence, the reverse saturation current density (J_O) can be expressed as follows (Li, 1993):

$$J_0 = qn_i^2 D_p / L_p N_D \tag{5}$$

where D_p and L_p are the minority carrier diffusion coefficient and diffusion length in the substrate region, respectively.

The relationship between V_{oc} and J_O is given as follows (Li, 1993):

$$V_{oc} = kT/q \ln(J_{sc}/J_0 + 1) \tag{6}$$

When J_{sc} is much higher than J_O, formula 6 can be simplified as follows (Li, 1993):

$$V_{oc} = kT/q \ln(J_{sc}/J_0) \tag{7}$$

With the increase in temperature, V_{oc} primarily depended on J_O because of the marginal variation in J_{sc} analyzed above. J_O is proportional to the square of n_i, which increases exponentially as the temperature increases. Therefore, J_O will increase significantly with the increase in temperature, resulting in the decrease of V_{oc}. Moreover, n_i depends on E_g and can be expressed as follows (Li, 1993).

$$n_i = N_c N_v \exp(-E_g/kT) \tag{8}$$

where N_c and N_v refer to the effective density of states of conduction band bottom and valence band bottom, respectively. The decrease in E_g increases n_i, leading to a further decline in V_{oc} and consequently a decrease in P_{max} and *FF*.

The ratio J_{sc}/J_O directly affects the law of V_{oc} variation with temperature (Liu et al., 2014a; Liu et al., 2014b). When the ratio J_{sc}/J_O is large, V_{oc} is a linearly decreasing function of temperature; in contrast, when the ratio J_{sc}/J_O is small, V_{oc} is an exponentially decreasing function of temperature. The prepared betavoltaics have high surface recombination rate, and this leads to a low J_{sc}/J_O, especially at high temperature range. Therefore, the T–V_{oc} and T–P_{max} curves in Figs. 9b and 9c were linear at low temperature and exponential at high temperature. Large activity density source produces high J_{sc} and high J_{sc}/J_O. This is why the linear temperature range of the monolayer betavoltaics irradiated by 4.90 mCi/cm^2 ^{63}Ni was slightly larger than that irradiated by 1.96 mCi/cm^2 ^{63}Ni. In the theoretical calculation, neither surface recombination nor volume recombination was considered, except radiative recombination, thus resulting in a high J_{sc}/J_O ratio and the consequent linear relationship of T–V_{oc} and T–P_{max}.

Because of the shunt resistance (R_{sh}) (Chandrashekhar et al., 2007; Singh et al., 2012; Singh et al., 2008), the measured V_{oc} sensitivities of monolayer and interbedded betavoltaics are lower than their corresponding calculated values. The radiation generated current flows more toward R_{sh} as R_{sh} decreases because of the shunting effect, resulting in a decrease in V_{oc} sensitivity. When R_{sh} is so small, no radiation-generated

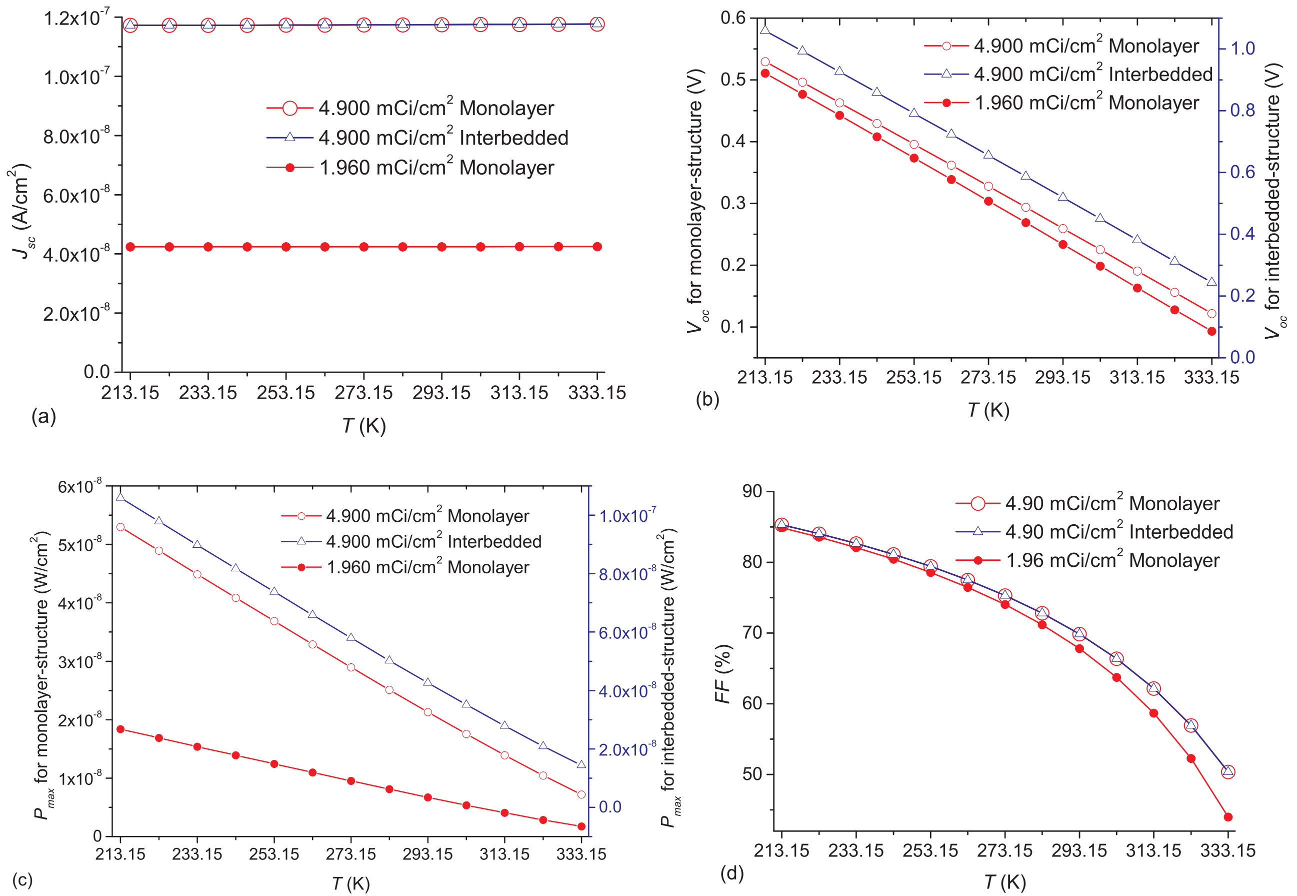

Fig. 10. Calculated changes in (a) J_{sc}, (b) V_{oc}, (c)P_{max}, and (d) FF as a function of temperature for the monolayer and interbedded betavoltaics irradiated by different activity densities of ^{63}Ni, respectively.

Table 7
Measured and calculated V_{oc} and P_{max} sensitivities of the upper, lower, and interbedded betavoltaic irradiated by 4.90 mCi/cm^2 bidirectional ^{63}Ni.

Results	ECUs	V_{oc} (mV/K)	P_{max} (%/K)
Measured sensitivity	Upper	−2.170	−1.143
	Lower	−2.230	−1.132
	Interbedded in series	−4.400	−1.137
Calculated sensitivity	Upper or lower	−3.399	−0.720
	Interbedded in series	−6.798	−0.720

Table 8
Measured and calculated V_{oc} and P_{max} sensitivities of the monolayer-structure betavoltaic irradiated by 1.96 mCi/cm^2 one-sided ^{63}Ni.

Results	V_{oc} (mV/K)	P_{max} (%/K)
Measured sensitivity	−2.490	−1.348
Calculated sensitivity	−3.482	−0.754

current pass the load circuit but R_{sh}, thus leading to a V_{oc} sensitivity of 0 mV/K (Chandrashekhar et al., 2007). The calcultion model assumed R_{sh} infinite and did not consider its effect, while the prepared betavoltaic has lower R_{sh} due to the leakage current. The R_{sh} value was estimated from the slope of the measured I–V curve at $V = 0$ and can be expressed as follows:

$$R_{sh} = \left.\frac{dV}{dI}\right|_{V=0, I=I_{sc}} \tag{9}$$

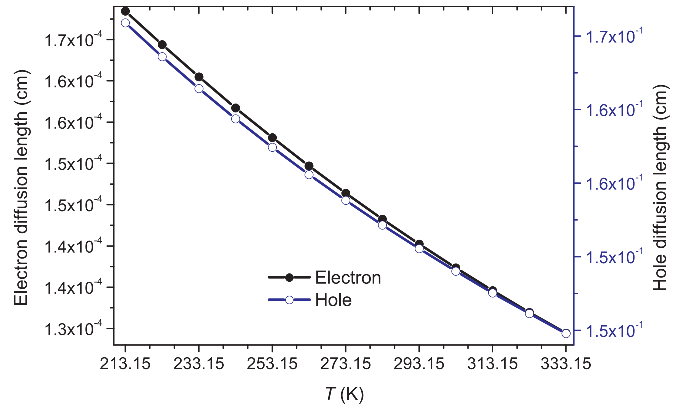

Fig. 11. Minority diffusion length as a function of temperature.

For example, the shunt resistances of the upper and lower monolayer betavoltaics with 4.90 mCi/cm^2 ^{63}Ni were 1.53 × 10^7 and 1.46 × 10^7 Ω, respectively; the R_{sh} of the lower monolayer betavoltaic with 1.96 mCi/cm^2 ^{63}Ni was 4.33 × 10^7 Ω at 293.15 K.

Substituting formulas 2 and 5 into formula 7, we get

$$V_{oc} = \frac{kT}{q}\left\{\ln\frac{J_{sc}N_D}{q\sqrt{D_p/\tau_p}} - \ln\frac{(5.29\times10^{19})^2}{300^{5.08}} - 5.08\ln T + \frac{13452}{T}\right\} \tag{10}$$

where τ_p is the minority carrier lifetime in the substrate region. The derivation of formula 10 gives the V_{oc} sensitivity, and then, formula 3

can be modified as follows:

$$\frac{dV_{oc}}{dT} = -\left(\frac{k}{q}\ln\frac{(5.29\times10^{19})^2}{300^{5.08}} + \frac{5.08k}{q}(\ln T + 1) - \frac{k}{q}\ln\frac{J_{sc}N_D}{q\sqrt{D_p/\tau_p}}\right) \tag{11}$$

FF is a function of temperature and can be expressed as follows (Honsberg and Bowden, 2014):

$$\frac{1}{FF}\frac{dFF}{dT} \approx \frac{1}{V_{oc}}\frac{dV_{oc}}{dT} - \frac{1}{T} \tag{12}$$

Substituting formula 12 into formula 4, P_{max} sensitivity can be obtained as follows:

$$\frac{1}{P_{\max}}\frac{dP_{\max}}{dT} \approx 2\cdot\frac{1}{V_{oc}}\frac{dV_{oc}}{dT} - \frac{1}{T} + \frac{1}{J_{sc}}\frac{dJ_{sc}}{dT} \tag{13}$$

Because the effect of temperature on J_{sc} is significantly less, the third term in the right hand side of formula 13 can be ignored. Thus,

$$\frac{1}{P_{\max}}\frac{dP_{\max}}{dT} \approx 2\cdot\frac{1}{V_{oc}}\frac{dV_{oc}}{dT} - \frac{1}{T} \tag{14}$$

If the ECU is certain, N_D is a constant, and the temperature dependences of D_p, L_p, and J_0 show similar changes for the betavoltaics irradiated by different radioisotope sources. At that time, the V_{oc} sensitivity depends on J_{sc}. High apparent activity density source results in high J_{sc} and consequently large V_{oc}, which lead to low V_{oc} and P_{max} sensitivities, as shown in formulas 13 and 14. As shown in Figs. 4a and 5a, J_{sc} increased as the thickness and apparent activity density of ^{63}Ni increased, which resulted in a decrease in V_{oc} and P_{max} sensitivities, as shown in Tables 5, 6, respectively. When the apparent activity density was certain, high average energy resulted in a high J_{sc}, leading to low V_{oc} and P_{max} sensitivities. In the experiment, J_{sc} of the betavoltaic with 4.90 mCi/cm^2 ^{63}Ni was higher than that of the betavoltaic with 1.96 mCi/cm^2 ^{63}Ni; hence, the V_{oc} and P_{max} sensitivities of the former were lower than those of the latter. From the above analysis, the higher the source thickness, activity density, and average energy, the lower is the betavoltaic performance responds to the temperature. To take advantage of this feature, we should choose thin, low activity density, and low average energy radioisotope source, when the betavoltaic is applied to temperature sensor especially at low temperature environment.

In addition, the V_{oc} in the experiment was much lower than that in the calculation due to the large leakage current of the prepared betavoltaic. This implies that the measured $1/V_{oc}$ in the first part on the right of formula 14 is much higher than the calculated one. Hence, although the measured V_{oc} sensitivity was less than the calculated one, the measured P_{max} sensitivity was greater than the calculated one. As shown in Fig. 6, the leakage current of the upper betavoltaic was higher than that of the lower one, thus resulting in a higher P_{max} sensitivity for the former (Table 7). This result indicates that the leakage current should be cut down to weaken the P_{max} temperature dependence.

5. Conclusion

In this paper, the effects of temperature on the ^{63}Ni–Si betavoltaic irradiated by beta source with different conditions were studied theoretically at a temperature range of 170–340 K. The temperature dependences of the monolayer and interbedded betavoltaics were measured at 213.15–333.15 K. The effects of apparent activity density were confirmed in the experiment. As the temperature was increased, the J_{sc} increased moderately, V_{oc} and P_{max} declined linearly, and FF decreased. The calculated results revealed that the higher the thickness, activity density, and average energy of the source, the lower is the betavoltaic performance responds to the temperature. With the increase in temperature, the V_{oc} and P_{max} of the upper, lower, and interbedded ^{63}Ni–Si betavoltaics decreased linearly at low temperature and decreased exponentially at high temperature in the experiment. For 4.90 mCi/cm^2 ^{63}Ni, the V_{oc} sensitivities of the three betavoltaics were –2.170, –2.230, and −4.40 mV/K; the P_{max} sensitivities were −1.143%, −1.132%, and −1.137%, respectively. The measured results confirmed that both the V_{oc} and P_{max} sensitivities of the lower monolayer betavoltaic with 4.90 mCi/cm^2 ^{63}Ni were lower than those, which are −2.490 mV/K and −1.348%, respectively, of the betavoltaic with 1.96 mCi/cm^2 ^{63}Ni. Moreover, because of low R_{sh} and high leakage current, the prepared monolayer and interbedded betavoltaics had lower V_{oc} sensitivities and higher P_{max} sensitivities compared to the calculated results. The leakage current should be cut down to weaken the P_{max} temperature dependence. Moreover, the measured V_{oc} sensitivity of the interbedded betavoltaic in series was equal to the sum of those of the upper and lower monolayer ones as predicted. Furthermore, the measured P_{max} sensitivity of the interbedded one was equal to the average of those of two monolayer ones. This work will help us understand the temperature dependence of betavoltaics better. Further studies will be conducted to show the whole picture of the betavoltaic temperature characteristics.

Acknowledgment

This work was supported by the National Natural Science Foundation of China (Grant No. 11505096 and 11675076), the National Defense Basic Scientific Research Project (Grant No. JCKY2016605C006), the Natural Science Foundation of Jiangsu Province (Grant No. BK20150735), the Shanghai Aerospace Science and Technology Innovation Project (Grant No. SAST2016112), the Priority Academic Program Development of Jiangsu Higher Education Institutions, and the Fundamental Research Funds for the Central Universities (Grant No. NJ20160031).

References

Adams, T., Revankar, S.T., Cabauy, P., Elkind, B., Cheu, D., 2016. Betavoltaic performance under extreme temperatures. Nucl. Technol. Radiat. Prot. 31 (4), 356–360.
Butera, S., Lioliou, G., Krysa, A.B., Barnett, A.M., 2016. Temperature dependence of an AlInP ^{63}Ni betavoltaic cell. J. Appl. Phys. 120 (14), 144501.
Butera, S., Lioliou, G., Barnett, A.M., 2017a. Temperature effects on gallium arsenide ^{63}Ni betavoltaic cell. Appl. Radiat. Isot. 125, 42–47.
Butera, S., Whitaker, M.D.C., Krysa, A.B., Barnett, A.M., 2017b. Investigation of a temperature tolerant InGaP (GaInP) converter layer for a ^{63}Ni betavoltaic cell. J. Phys. D: Appl. Phys. 50, 345101.
Butera, S., Whitaker, M.D.C., Krysa, A.B., Barnett, A.M., 2017c. Temperature effects on an InGaP (GaInP) 55Fe X-ray photovoltaic cell. Sci. Rep. 7, 4981.
Chandrashekhar, M.V.S., Duggirala, R., Spencer, M.G., Lal, A., 2007. 4H SiC betavoltaic powered temperature transducer. Appl. Phys. Lett. 91 (5), 053511.
Chen, C.-C., Chang, Y.-Y., Zhang, J.-W., 2012. A novel betavoltaic microbattery based on SWNTs thin film-silicon heterojunction. In: 2012 Proceedings of the 25th International Conference on Micro Electro Mechanical Systems (MEMS). IEEE, Paris, 2012, pp 1197–1200.
Cheu, D.S., Adams, T.E., Revankar, S.T., 2017. Experiments and modeling on effects of temperature on electrical performance of a betavoltaic. Nucl. Eng. Des. http://dx.doi.org/10.1016/j.nucengdes.2017.06.028.
Ghasemi, N.G.R., Rahmani, F., Abaeiani, G.R., 2014. Design and optimization of beta-cell temperature sensor based on ^{63}Ni-Si. Appl. Radiat. Isot. 86 (0), 46–51.
Honsberg, C., Bowden, S., 2014. Effect of temperature. Opgeroepen Op. 3, 19.
Klaassen, D.B.M., 1992. A unified mobility model for device simulation—II. temperature dependence of carrier mobility and lifetime. Solid-State Electron. 35 (7), 961–967.
Li, S.S., 1993. Semiconductor Physical Electronics. Plenum Press, New York.
Liu, Y.-P., Tang, X.-B., Xu, Z.-H., Hong, L., Chen, D., 2014a. Experimental and theoretical investigation of temperature effects on an interbedded betavoltaic employing epitaxial Si and bidirectional ^{63}Ni. Appl. Radiat. Isot. 94, 152–157.
Liu, Y.-P., Tang, X.-B., Xu, Z.-H., Hong, L., Wang, P., Chen, D., 2014b. Optimization and temperature effects on sandwich betavoltaic microbattery. Sci. China Technol. Sci. 57 (1), 14–18.
Liu, Y.-P., Tang, X.-B., Xu, Z.-H., Hong, L., Wang, H., Liu, M., Chen, D., 2015. Influences of planar source thickness on betavoltaics with different semiconductors. J. Radioanal. Nucl. Chem. 304 (2), 517–525.
Liu, Y.-P., Xu, Z.-H., Wang, H., Tang, X.-B., 2017. Vacuum degree effects on betavoltaics irradiated by ^{63}Ni with different apparent activity densities. Sci. China Technol. Sci. 60 (2), 282–288.
Luo, S.-Z., Wang, G.-Q., Zhang, H.-M., 2011. Advance in radiation-voltaic isotope battery. J. Isot. 24 (1), 3–13. http://dx.doi.org/10.7538/tws.2011.24.01.0001.
Misiakos, K., Tsamakis, D., 1993. Accurate measurements of the silicon intrinsic carrier density from 78 to 340 K. J. Appl. Phys. 74 (5), 3293–3297.
Olsen, L.C., Cabauy, P., Elkind, B.J., 2012. Betavoltaic power sources. Phys. Today 65 (12), 35–38.

Reggiani, S., Valdinoci, M., Colalongo, L., Rudan, M., Baccarani, G., 2000. An analytical, temperature-dependent model for majority-and minority-carrier mobility in silicon devices. VLSI Des. 10 (4), 467–483.

Singh, P., Ravindra, N.M., 2012. Temperature dependence of solar cell performance - an analysis. Sol. Energy Mater. Sol. Cells 101, 36–45.

Singh, P., Singh, S.N., Lal, M., Husain, M., 2008. Temperature dependence of *I–V* characteristics and performance parameters of silicon solar cell. Sol. Energy Mater. Sol. Cells 92 (12), 1611–1616.

Wang, G.-Q., Hu, R., Wei, H.-Y., Zhang, H.-M., Yang, Y.-Q., Xiong, X.-L., Liu, G.-P., Luo, S.-Z., 2010. The effect of temperature changes on electrical performance of the betavoltaic cell. Appl. Radiat. Isot. 68 (12), 2214–2217.

Wang, H., Tang, X.-B., Liu, Y.-P., Xu, Z.-H., Liu, M., Chen, D., 2015. Temperature effect on betavoltaic microbatteries based on Si and GaAs under ^{63}Ni and ^{147}Pm irradiation. Nucl. Instrum. Methods Phys. Res. Sect. B, Beam Interact. Mater. At. 359, 36–43.